1682 *Biochemistry* **2011,** *50,* 1682–1690
DOI: 10.1021/bi101474v

BIOCHEMISTRY
including biophysical chemistry & molecular biology
Article

Making Structural Sense of Dimerization Interfaces of Delta Opioid Receptor Homodimers[†]

Jennifer M. Johnston,[‡,⊥] Mahalaxmi Aburi,[⊥,§] Davide Provasi,[‡] Andrea Bortolato,[‡] Eneko Urizar,[§] Nevin A. Lambert,[∥] Jonathan A. Javitch,[§] and Marta Filizola*[,‡]

[‡]*Department of Structural and Chemical Biology, Mount Sinai School of Medicine, New York, New York 10029, United States,* [§]*Center for Molecular Recognition and Departments of Psychiatry and Pharmacology, College of Physicians and Surgeons, Columbia University, New York, New York 10032, United States, and* [∥]*Department of Pharmacology and Toxicology, Medical College of Georgia, Augusta, Georgia 30912, United States.* [⊥]*These authors contributed equally to this work.*

Received September 10, 2010; Revised Manuscript Received January 24, 2011

ABSTRACT: Opioid receptors, like other members of the G protein-coupled receptor (GPCR) family, have been shown to associate to form dimers and/or oligomers at the plasma membrane. Whether this association is stable or transient is not known. Recent compelling evidence suggests that at least some GPCRs rapidly associate and dissociate. We have recently calculated binding affinities from free energy estimates to predict transient association between mouse delta opioid receptor (DOR) protomers at a symmetric interface involving the fourth transmembrane (TM4) helix (herein termed "4" dimer). Here we present disulfide cross-linking experiments with DOR constructs with cysteines substituted at the extracellular ends of TM4 or TM5 that confirm the formation of DOR complexes involving these helices. Our results are consistent with the involvement of TM4 and/or TM5 at the DOR homodimer interface, but possibly with differing association propensities. Coarse-grained (CG) well-tempered metadynamics simulations of two different dimeric arrangements of DOR involving TM4 alone or with TM5 (herein termed "4/5" dimer) in an explicit lipid−water environment confirmed the presence of two structurally and energetically similar configurations of the 4 dimer, as previously assessed by umbrella sampling calculations, and revealed a single energetic minimum of the 4/5 dimer. Additional CG umbrella sampling simulations of the 4/5 dimer indicated that the strength of association between DOR protomers varies depending on the protein region at the interface, with the 4 dimer being more stable than the 4/5 dimer.

Opioid receptors (ORs)[1] are members of the G protein-coupled receptor (GPCR) superfamily. They play a major role in the control of nociceptive pathways, but they also modulate neuroendocrine physiology, mood, stress, appetite, immune responses, and autonomic functions, including respiration and thermoregulation. On the basis of radioligand binding profiles, ORs can be classified into three major subtypes: mu (MOR), delta (DOR), and kappa (KOR) receptors (*1*). Like several other members of the GPCR family (*2*), opioid receptors have been shown to interact among themselves at the plasma membrane to form dimers and/or oligomers (*3*−*11*). However, the extent to which these interactions are stable and/or specific is unknown.

Prevailing views about the static nature of GPCR dimers have recently been challenged by compelling evidence from imaging studies. A recent single-molecule study using total internal reflection fluorescence microscopy showed transient formation of a typical family A GPCR, the M1 muscarinic acetylcholine receptor, in living cells, on the time scale of 1 s (*12*). Recent fluorescence recovery after photobleaching (FRAP) studies of β1-adrenoceptors (*13*) and dopamine D2 receptors (*14*) also were consistent with interactions of these GPCRs being transient.

Using experimental measurements of the diffusion coefficient of a protomeric opioid receptor (*15*), along with free energies reconstructed from umbrella sampling of DOR dimers involving TM4 centered at residue V181$^{4.58}$ [where the superscript refers to the Ballesteros−Weinstein generic numbering scheme (*16*)], we were recently able to calculate the association rate and dimerization constant of so-called "4" dimers of DOR (*17*). These calculated values allowed us to estimate a lifetime of ∼4.4 s for DOR dimers within an explicit palmitoyloleoylphosphatidylcholine (POPC)/10% cholesterol/water environment (*17*), in rough agreement with single-molecule experimental values obtained for the M1 muscarinic receptor (*12*).

Although the degree of specificity of these interactions and the underlying mechanisms [e.g., conserved motifs or hydrophobic mismatch? (*18*)] are not known, the proposed short life span of

[†]This work was supported by National Institutes of Health Grants DA020032 and DA026434 (to M.F.), GM078319 and GM096762 (to N.A.L.), and DA022413 (to J.A.J.). The computations were supported in part by the National Science Foundation through TeraGrid advanced computing resources provided by TRAC MCB080077. A.B. was supported in part by a 2008−2009 American-Italian Cancer Foundation Post-Doctoral Research Fellowship.

*To whom correspondence should be addressed. E-mail: marta.filizola@mssm.edu. Telephone: (212) 659-8690. Fax: (212) 849-2456.

[1]Abbreviations: BRET, bioluminescence resonance energy transfer; CG, coarse-grained; COM, center of mass; CV, collective variable; D2R, dopamine D2 receptor; DOR, delta opioid receptor; FES, free energy surface; FRAP, fluorescence recovery after photobleaching; GPCR, G protein-coupled receptor; GRK3, G protein-coupled receptor kinase 3; KOR, kappa opioid receptor; MD, molecular dynamics; MOR, mu opioid receptor; OR, opioid receptor; TM, transmembrane; PBS, phosphate-buffered saline; PEI, polyethylenimine; POPC, palmitoyloleoylphosphatidylcholine; rmsd, root-mean-square deviation; WHAM, Weighted Histogram Analysis Method; WT, wild-type.

 Published on Web 01/24/2011

DOR homodimers could still be sufficient for them to exert unique pharmacological functions. Thus, understanding in detail the interaction between DOR protomers is extremely important, because it might inform the rational design of novel selective analgesic drugs targeting oligomeric receptors.

Here, we have investigated possible interfaces in DOR homodimeric complexes by means of an integrated experimental−computational approach aimed at selecting energetically favorable dimeric models among all different possibilities amenable to TM4 or TM5 helices. Our focus on these helices was based on a large body of literature suggesting a direct primary involvement of lipid-exposed surfaces of TM4 and/or TM5 in the dimerization/oligomerization interfaces of several GPCRs, in particular: dopamine D2 receptor (D2R) homodimer (*19*−*22*), serotonin 5-HT4 receptor homodimer (*23*), serotonin 5-HT2C homodimer (*24*), α1b-adrenoceptor homodimer (*25*, *26*), C5a receptor homodimer (*27*), chemokine CCR5 homodimer (*28*), serotonin 5-HT2A-metabotropic glutamate receptor 2 heterodimer (*29*), secretin (*30*), and corticotropin releasing hormone-VT2 arginine vasotocin receptor heterodimer (*31*). We performed bioluminescence resonance energy transfer (BRET) experiments to confirm DOR interactions in our experimental system, as well as subsequent cross-linking experiments on DOR constructs with substituted cysteines at the extracellular ends of TM4 and TM5. Since the DOR homodimer interface could not be defined unambiguously on the basis of the few contact points implied by experiments, we conducted Gaussian-biased MD simulations to obtain free energy estimates of all possible dimeric configurations around those specific contact points and to ensure that identified lowest-energy minima represent the most favorable energetic configurations satisfying the experimental constraints. Specifically, guided by the experimental results, we conducted coarse-grained (CG) well-tempered metadynamics simulations of pairs of mouse DOR protomers facing one another at the identified cross-linking positions in TM4 or TM5 within an explicit lipid−water environment. Using reaction coordinates that describe the relative position of the interacting protomers, we have explored alternative 4 or "4/5" dimeric arrangements of DOR centered at these specific positions and identified their most favorable energetic minima. Finally, CG umbrella sampling simulations of the 4/5 dimer were conducted to assess the stability of this association compared to the association of the 4 dimer (*17*).

MATERIALS AND METHODS

Receptor Constructs and Transfection. For cross-linking experiments, cysteine mutations were generated in the wild-type (WT) mouse DOR, epitope-tagged at the N-terminus with a signal peptide followed by a Myc tag (*32*). Mutations were confirmed by DNA sequencing, subcloned into the pcDNA5/FRT/TO expression vector (Invitrogen), and stably expressed in Flp-In T-REx HEK293 cells as described previously (*32*). For BRET experiments, DOR, C-terminally tagged with either full-length mVenus or Renilla Luciferase 8 (RLuc8), was subcloned in the pcDNA 3.1 expression vector, sequenced, and transiently transfected in HEK293T cells using polyethylenimine (PEI) (Polysciences Inc.) (*22*). Experiments were performed 48 h post-transfection.

G protein-coupled receptor kinase 3 (GRK3) constructs contained amino acids G495−L688 of bovine GRK3 (NP_776925; also known as β-adrenergic receptor kinases 2 or βARK2), preceded by a myristic acid attachment peptide (mas; MGSSKSKTSNS) (masGRK3-ct). The stop codon of GRK3 was replaced with a GGG linker, which was followed by Rluc8 (*33*). $G\gamma_2$-V was expressed by a plasmid encoding amino mVenus fused to a GGSGGG linker and the N-terminus of human $G\gamma_2$. The BRET donor and acceptor, masGRK3-ct-RluC8 and $G\gamma_2$-V, respectively, were transiently cotransfected with $G_{\alpha i1}$ and $G_{\beta 1}$ along with the DOR (WT or the specified mutants) using PEI. BRET-based activation experiments were performed 48 h post-transfection.

BRET. The BRET experiments were performed with cells in suspension and were quantified with a Pherastar (BMG) (*22*). Briefly, BRET titration experiments were performed with cells coexpressing a constant amount of DOR-RLuc8 and increasing amounts of DOR-mVenus. The BRET signal was determined by quantifying and calculating the ratio of the light emitted by mVenus (510−540 nm) over that emitted by RLuc8 (485 nm) for BRET. The net BRET values were obtained by subtracting the background from cells expressing RLuc8 alone. BRET competition experiments were performed in the presence of untagged receptor that was coexpressed with DOR-RLuc8 and DOR-mVenus in HEK293 T cells (*22*). Activation assays were performed as described with the agonist SCN-80 (*33*).

Binding. Whole cells stably expressing the specified DOR construct were suspended in 1 mL of buffer A [25 mM HEPES, 140 mM NaCl, 5.4 mM KCl, 1 mM EDTA, and 0.006% bovine serum albumin (pH 7.4)]. Cells were diluted 50-fold with buffer A. [^{3}H]Naltrindole (Perkin-Elmer) binding was performed in duplicate 1.1 mL microtube strips with eight different concentrations of [^{3}H]naltrindole between 50 and 1000 pM in buffer A with 100 μL of the cell suspension in a final volume of 250 μL. The mixture was incubated at room temperature for 4 h and then filtered using a Brandel cell harvester through Whatman 934AH glass fiber filters (Brandel) pretreated with 0.2% PEI. The filter was washed twice with 1 mL of 10 mM Tris-HCl and 120 mM NaCl (pH 7.4). Nonspecific [^{3}H]naltrindole binding was assessed in the presence of 10 μM naloxone. The data were fit to a saturation binding curve using nonlinear regression analysis in GraphPad Prism.

Flow Cytometry Analysis. To assess the surface expression of each receptor construct, flow cytometry analysis was performed on WT or mutants stably expressed in Flp-In T-REx HEK293 cells using an Accuri C6 Flow Cytometer system (Accuri Cytometers). The cells were harvested 48 h post-transfection, washed, and resuspended in phosphate-buffered saline (PBS). Cells were incubated at room temperature for 30 min with a monoclonal anti-Myc antibody (1:500) (Hybridoma Facility, Mount Sinai, NY), washed, and incubated with a secondary anti-mouse antibody labeled with Alexa Fluor-(AF) 647 (1:500) (Invitrogen) on ice. Analysis was based on light scatter, and fluorescence signals produced from laser illumination at 640 nm. Signals corresponding to forward and side scatter and fluorescence were accumulated; the fluorescence signals were screened using FL-4 (675 nm filter). Threshold levels were set to eliminate detection of cell debris; 10000 events were collected at the medium rate setting.

Cross-Linking. The cross-linking reagents $CuSO_4$ and 1,10-phenanthroline (CuP) in a 1:3 molar ratio or mercuric chloride ($HgCl_2$) were applied to intact adherent Flp-In T-REx HEK293 cells stably expressing the indicated cysteine mutants for 10 min at 25 °C. Cross-linking was conducted after induction of receptor expression with 1 μg/mL tetracycline overnight. The cross-linking reaction was stopped by washing the cells twice with PBS

followed by the addition of 20 mM *N*-ethylmaleimide (NEM). The cells were harvested and extracted (*21*). Twenty micrograms of protein was loaded per sample, and sodium dodecyl sulfate−polyacrylamide gel electrophoresis (SDS−PAGE) and immunoblotting using the anti-Myc rabbit polyclonal antibody (1:800, Santa Cruz Biotechnology) were performed (*21*).

Molecular Modeling. In the absence of available crystal structures of opioid receptors, molecular modeling was employed to generate all-atom structural models of DOR protomers from *Mus musculus*, using the same strategy we recently reported in the literature for human DOR (*34*). Briefly, we built the TM region of mouse DOR by homology modeling using the crystal structure of the β2 adrenergic receptor at 2.4 Å resolution (Protein Data Bank entry 2RH1) (*35*), and a sequence alignment based on conserved residues and motifs that are present in family A GPCRs as inputs to Modeler 9v3 (*36*). The loop regions were built ab initio using Rosetta 2.2 (*37*), and the procedure described in ref *34*. The protein N-terminus (residues 1−44) and C-terminus (residues 335−372) were not included in the models. Pairs of the resultant DOR models were placed facing one another at putative symmetrical interfaces involving TM4 and residue V181$^{4.58}$ (the 4 dimer) or TM4 and TM5 and residue T213$^{5.38}$ (the 4/5 dimer).

Residues in this work are identified according to their position in the mouse DOR sequence and, when appropriate, according to the Ballesteros−Weinstein N1.N2 notation (*16*), reported as a superscript. In this notation, the first number (N1) refers to the TM helix in question and the second number (N2) to the position of the residue in the sequence relative to the most conserved residue in the TM helix, which is assigned a value of 50.

Molecular Dynamics Simulations. The pairs of all-atom DOR models were converted to CG representations, as defined by the Martini CG force field (*38*, *39*), in which a single bead represents approximately four heavy atoms. To maintain the integrity of the secondary structure of the CG protomers, an internal elastic network was applied to the backbone beads of each residue, according to their secondary structure, as described in ref *17*.

All simulations were performed using GROMACS version 4.0.5 (*40*) with the Plumed plug-in (*41*). The CG dimers were embedded in a CG POPC membrane patch containing 10% cholesterol. This membrane patch had previously been allowed to self-assemble, over a period of 100 ns, from a box containing randomly oriented CG POPC, cholesterol, and water beads, in a manner similar to that described in ref *17*. Each of the CG DOR dimers was embedded in this membrane using the inflation−deflation protocol as described by Tieleman and colleagues (*42*). Receptors were oriented such that the vector joining their centers of mass (COM) was along the diagonal of the membrane plane to maximize the space available for subsequent rearrangement of the protomers. The DOR pairs and the membrane were then solvated, and counterions were added to neutralize the systems. These systems were energy minimized and equilibrated by performing cycles of molecular dynamics (MD) under successively relaxed position restraints (1000, 100, 10, and 0 kJ mol^{-1} nm^{-2}) for a total of 10 ns. Each of the unrestrained systems was then simulated for an additional 50 ns, and their equilibration was checked by monitoring the root-mean-square deviation (rmsd) of the TM regions of the proteins.

Metadynamics Simulations. The free energy surface for each of the two putative dimer interfaces of DOR involving TM4 with or without TM5 (termed 4/5 and 4 dimers, respectively) was investigated using well-tempered metadynamics simulations (*43*).

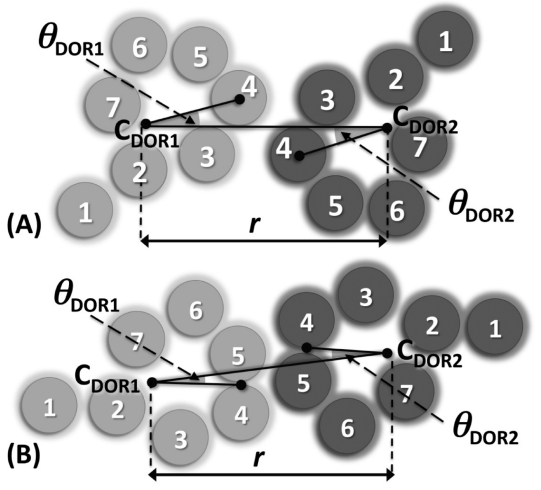

FIGURE 1: Reaction coordinates used to describe the relative position of interacting protomers DOR1 and DOR2 during simulation, superimposed on schematic representations of the (A) 4 and (B) 4/5 dimeric arrangements of DOR. Each circle represents a TM helix, and the two protomers are distinguished by different shades of gray. The relative position of the two protomers was described by (i) the distance r between the COMs (C_{DOR1} and C_{DOR2}) of the two TM regions of protomers DOR1 and DOR2, (ii) the rotational angle θ_{DOR1}, defined by the projection onto the plane of the membrane of the COM of TM4$_{DOR1}$ or TM4/5$_{DOR1}$, the C_{DOR1}, and the C_{DOR2}, and (iii) the equivalent rotational angle θ_{DOR2}.

The collective variable (CVs) used to describe the relative position of interacting protomers DOR1 and DOR2 during simulation are depicted in Figure 1A for the 4 dimer and in Figure 1B for the 4/5 dimer. Specifically, the relative position of the two protomers was described by (i) the distance r between the COMs (C_{DOR1} and C_{DOR2}) of the two TM regions of protomers DOR1 and DOR2, (ii) the rotational angle θ_{DOR1}, defined by the projection onto the plane of the membrane of the COM of TM4$_{DOR1}$ (or TM4/5$_{DOR1}$ for the 4/5 dimer), the C_{DOR1}, and the C_{DOR2}, and (iii) the equivalent rotational angle θ_{DOR2}. Angles were calculated as arccosines of the inner product of the normalized vectors connecting the projections onto the plane of the membrane of the COMs of TM4 (or TM4 and TM5), and the two helical bundles.

To aid simulation convergence, we restricted the rotational and translational movement of the entire DOR dimer relative to the simulation cell. Specifically, we applied harmonic restraining potentials centered at zero, with a force constant k of 200 kJ mol^{-1} nm^{-2}, to both the distance from the C_{DOR1} projection to the center of the $z = 0$ plane of the simulation box and the distance from the C_{DOR2} projection to the diagonal thereof.

Hills were applied only to the angle CVs (i.e., θ_{DOR1} and θ_{DOR2}). The initial height of the biasing Gaussians in the well-tempered metadynamics algorithm was set to 0.5 kJ/mol (~0.12 kcal/mol), with a bias factor of 15. To ensure a thorough exploration of the possible interfaces between two DOR dimers involving either residue V181$^{4.58}$ or T213$^{5.38}$ on a reasonable time scale, we limited the sampling of the two rotational angles, θ_{DOR1} and θ_{DOR2}, to an ~25° interval for simulations of the 4 dimer and to an ~17° interval for the simulations of the more constrained 4/5 dimer, using upper and lower steep repulsive restraining potentials. The starting values of the angles were as follows: $\theta_{DOR1} \sim 18°$ and $\theta_{DOR2} \sim 25°$ in the 4 dimer, and $\theta_{DOR1} \sim 26°$ and $\theta_{DOR2} \sim 22°$ in the 4/5 dimer. The upper and lower limits were set equidistant from these starting values. The values of

these parameters were chosen after an extensive grid search of parameter ranges (data not shown).

Two 1.5 μs well-tempered metadynamics simulations were performed, with a time step of 20 fs, for each of the two DOR homodimers, i.e., 4 or 4/5. Convergence of these simulations was assessed by monitoring the height of the biasing hills applied during simulation: this height decreases as the wells in the free energy surface are filled up, reaching a value of zero when the simulation is converged. Plots of the hill heights for the 4 and 4/5 dimers are shown in panels A and B of Figure S1 of the Supporting Information, respectively, and indicate that the hill heights are very close to zero after several hundred nanoseconds.

Periodic boundary conditions were employed, and electrostatic and van der Waals interactions were cut off and used in their shifted forms. Temperature and pressure were maintained by coupling to baths using the V-rescale (*44*) and Berendsen (*45*) algorithms, respectively. A reference temperature of 300 K and a coupling constant of 1 ps were used for the V-rescale algorithm, and the Berendsen algorithm employed a coupling constant of 2 ps to a reference pressure of 1 bar.

Conversion of Lowest-Energy CG Structures to All-Atom Representations. We used the method of Rzepiela and colleagues (*46*) to convert the lowest-energy structures of the 4 and 4/5 dimers of DOR from each of the CG metadynamics simulations back to an atomistic representation. This method employs a simulated annealing MD simulation in which the CG and atomistic structures are coupled via restraints. The resulting all-atom structures were then embedded into a pre-equilibrated all-atom membrane and solvated in a fashion similar to that described above for the CG systems and as in ref *42*. These systems were energy minimized and equilibrated by performing cycles of MD under successively relaxed position restraints (1000, 100, 10, and 0 kJ mol^{-1} nm^{-2}) for a total of 10 ps. A further 1 ns of unrestrained simulation was used, and analysis of interprotomer contacts was performed on these systems. This multiscale approach allows us to consider atomic details of side chain interactions that are not well resolved in the CG simulations.

Umbrella Sampling Simulations. Simulations of the 4/5 dimer of DOR with the interacting protomers at different distances were performed according to the protocol described in detail in ref *17*. To keep the exploration to 4/5 dimeric configurations of DOR exhibiting symmetric contacts between residues at position 5.38, the two rotational angles, θ_{DOR1} and θ_{DOR2}, were constrained to an ~17° interval around their centers by steep repulsive potentials, in a manner similar to the metadynamics simulations described above. The Weighted Histogram Analysis Method (WHAM) code from the Grossfield Lab (http://membrane.urmc.rochester.edu/content/wham) was used to derive the free energy from these simulations as a function of the distance between the COMs of the protomers.

Thermodynamics and Kinetics. The dimerization constant of the 4/5 dimer of DOR in a POPC/10% cholesterol/water environment was calculated using the free energy estimates resulting from the umbrella sampling simulations, and an approach originally described by Roux and co-workers (*47*−*49*). We recently used this approach to predict the dimerization constant of the 4 dimer of DOR and reported the details of its formulation elsewhere (*17*). The dimerization constant of the 4/5 dimer of DOR calculated here was then used to calculate the dissociation rate and average lifetime of this particular conformational arrangement. The equations used to calculate these values are reported in detail elsewhere (*17*).

RESULTS

Biophysical Evidence of DOR Dimerization. BRET was used to establish receptor interactions in our model system. BRET titration experiments were performed with HEK293T cells coexpressing constant amounts of DOR-RLuc8 and increasing concentrations of DOR-mVenus. A saturable BRET signal was observed for DOR−DOR (Figure S2A of the Supporting Information). In addition, BRET experiments were performed in the presence of untagged DOR, which inhibited the BRET signal by competing for dimerization with the receptors fused to the probes. Competition over the entire titration range rules out changes in the absolute or relative levels of expression of the BRET probes as the cause of the weakened BRET signal (Figure S2B of the Supporting Information). The BRET results are consistent with very close interactions between DOR protomers and with previous findings (*11*, *50*).

Cross-Linking of Substituted Cysteines at the Extracellular Ends of TM4 and TM5. To characterize the interfaces of DOR homodimers, we used cysteine cross-linking. Therefore, it was essential to develop a system in which the background receptor construct ran as a monomer on nonreducing SDS−PAGE despite treatment with sulfhydryl-specific cross-linking reagents. In preliminary experiments using stably expressed WT DOR, we used as cross-linking reagents CuP and $HgCl_2$. In other studies of membrane proteins, CuP was unable to cross-link cysteines deep in the transmembrane domain, whereas $HgCl_2$ efficiently cross-linked a group of these residues that were inferred to be at an oligomeric interface (*51*, *52*). Whereas treatment with CuP failed to alter the monomeric species of WT DOR, treatment with $HgCl_2$ resulted in a substantial amount of receptor migrating as a larger band of ~110 kDa (Figure 2A), consistent with the expected migration of a DOR homodimer that is disulfide cross-linked via an endogenous cysteine. In addition to the conserved C121$^{3.25}$−C198 disulfide bridge, six endogenous cysteine residues are present in DOR helices TM1 and TM4−TM7. Three cysteine residues in the extracellular regions of TM1 (C60$^{1.43}$), TM4 (C171$^{4.48}$), and TM5 (C216$^{5.41}$) were selected for mutation as they were lipid-exposed, and possibly involved in dimeric interfaces involving TM1, TM4, or both TM4 and TM5, as previously demonstrated for D2R (*21*, *22*).

Simultaneous mutation of all three of these cysteine residues to serine (C60$^{1.43}$S/C171$^{4.48}$S/C216$^{5.41}$S) resulted in a background construct (termed "pseudo-Cys-less") that migrated almost exclusively as a heterogeneously glycosylated monomer of ~52 kDa via nonreducing SDS−PAGE (Figure 2A) after treatment with either CuP or $HgCl_2$. To identify the cysteines that were cross-linked in WT DOR, we generated the double mutant constructs C60S$^{1.43}$S/C171$^{4.48}$S and C60$^{1.43}$S/C216$^{5.41}$S. Both of these constructs behaved like WT DOR, as their migration was unaltered by CuP, but they migrated as a dimer after treatment with 20 μM $HgCl_2$ (Figure 2A), indicating that each of the endogenous cysteines at positions 4.48 and 5.41 could be cross-linked by $HgCl_2$.

The pseudo-Cys-less (CL) construct was used for substituted cysteine analysis to map in greater detail the 4 and 4/5 interfaces. Several positions in TM4 and TM5 (including 4.56−4.63 and 5.38−5.40) were individually substituted with cysteine, and the constructs were subcloned into the pcDNA5/FRT/TO expression vector and stably expressed in Flp-In T-REx HEK293 cells.

Cross-linking experiments were performed as for the WT and background receptor constructs (Figure 2B). All of the

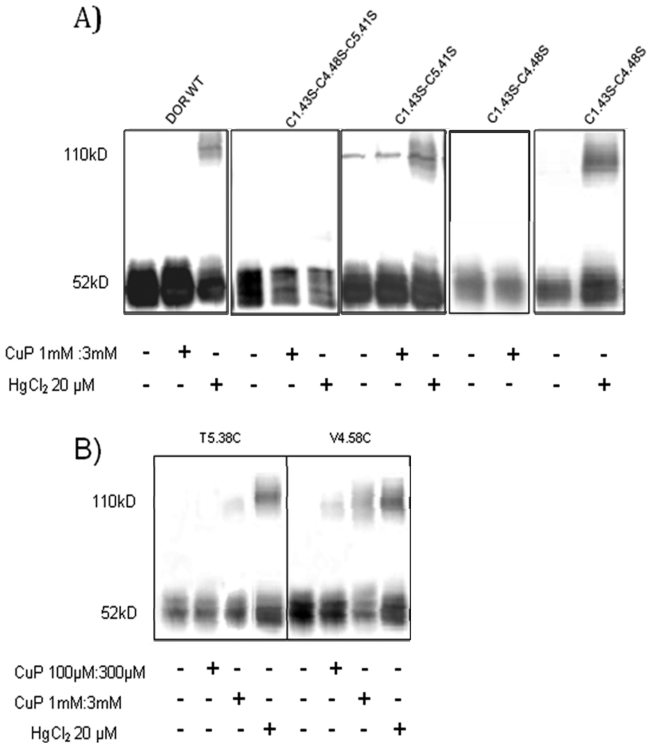

FIGURE 2: Cross-linking of DOR to a homodimer by copper phenanthroline (CuP) and mercuric chloride ($HgCl_2$). (A) Treatment of Myc-DOR and indicated mutant constructs with CuP or 20 μM $HgCl_2$. (B) Cross-linking of the DOR TM4 and TM5 cysteine mutant with CuP and 20 μM $HgCl_2$. Stably expressed cysteine mutants in TM4 and TM5 were cross-linked with CuP at 25 °C for 10 min, and the reaction was stopped with *N*-ethylmaleimide and analyzed by immunoblotting. All experiments were repeated at least three times, and a representative experiment is shown.

substituted cysteines in the CL background were expressed and led to a maturely glycosylated receptor, with the exception of P182$^{4.59}$C, I183$^{4.60}$C, V185$^{4.62}$C, and K214$^{5.39}$C. Flow cytometry analysis of the maturely glycosylated mutants showed robust surface expression (Figure S3 of the Supporting Information). Of these mutants, only V181$^{4.58}$C and T213$^{5.38}$C led to cross-linking with both CuP and $HgCl_2$ to a dimer band similar to that observed with WT DOR (Figure 2B). None of the other mutants were cross-linked by either reagent (data not shown; Table S1 of the Supporting Information). The extent of cross-linking of V181$^{4.58}$C, located at the extracellular end of TM4, was greater than that for T213$^{5.38}$C. A number of factors may contribute to this difference, including the local environment of the substituted cysteines, the distance or the orientation of these cysteines at a homodimer interface, and the stability of this interface.

We performed [^{3}H]naltrindole binding experiments to determine K_d and B_{max} values for WT and the CL background construct as well as the mutants that were cross-linked by CuP (CL, V181$^{4.58}$C, and T213$^{5.38}$C). These mutants bound [^{3}H]naltrindole with near-normal K_d and B_{max} values (Table S2 of the Supporting Information), consistent with the flow cytometry data described above (Figure S3 of the Supporting Information). The DOR agonist SNC-80 led to robust activation of the WT and key mutants, which was measured using a G protein BRET-based biosensor (*33*). The CL construct had a somewhat diminished potency and efficacy, which curiously was not seen in V181$^{4.58}$C and T213$^{5.38}$C, two mutations made in the CL background. Taken together, our data demonstrate that the key mutants express at the surface, bind the antagonist

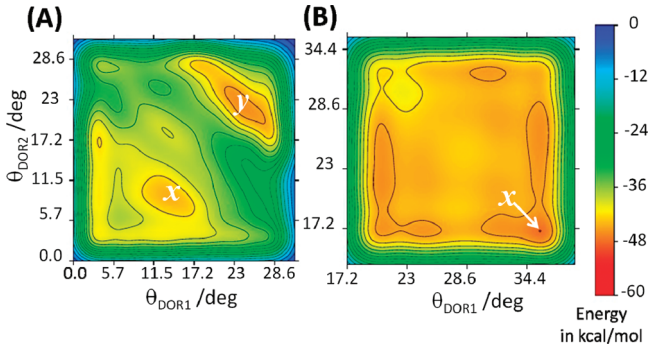

FIGURE 3: Free energy maps derived from the hills deposited during the well-tempered metadynamics simulations of the coarse-grained representations of the (A) 4 and (B) 4/5 interfaces. The axes represent the angles θ_{DOR1} and θ_{DOR2} as defined in the legend of Figure 1. Red denotes the lowest energy and blue the highest energy. Lowest-energy regions are highlighted with labels.

[^{3}H]naltrindole normally, and are activated by the agonist SNC-80, indicating that they are properly folded and interact appropriately with G proteins.

Molecular Characterization of the 4 and 4/5 Dimers of DOR. To select energetically favorable dimeric models of DOR homodimers among all different possibilities amenable to TM4 interfaces involving either position 4.58 or 5.38, we used enhanced sampling algorithms working within the framework of classical molecular dynamics. A flowchart of the modeling and simulation strategy is provided in Figure S4 of the Supporting Information. Specifically, we conducted well-tempered metadynamics simulations of both 4 and 4/5 dimers of DOR in the phase space defined by a small number of collective variables, applying a Gaussian bias to the angle CVs describing the relative orientation of the DOR protomers (see full CV definitions in Materials and Methods and Figure 1). To enable a thorough exploration for each dimer in a reasonable time scale, we also applied restraints to these CVs, as well as to the distance between protomers. Specifically, the distance restraint was chosen such that it limited the exploration to dimeric configurations of DOR (i.e., <3.4 nm between the COMs of the protomers), while the selected angle ranges for each of the putative DOR dimers limited the search to an ~25° interval around position 4.58 or an ~17° interval around position 5.38, to keep these positions within a range of physical interaction (Cβ distance of $\leq$12 Å).

Thorough exploration of the conformational space available to the interacting DOR protomers was verified by monitoring the evolution of the CVs during simulations. Panels A and B of Figure S5 of the Supporting Information show the evolution of the CVs for the 4 and 4/5 dimers, respectively. Because Gaussian bias was applied to the angle CVs (θ_{DOR1} and θ_{DOR2}), we can see good exploration of the angle ranges for both θ_{DOR1} and θ_{DOR2} during the simulations, as evidenced by repeated recrossing of the available phase space, as defined by the two limiting potentials (equivalent to ranges of ~25° and 15°, respectively).

The free energy surface (FES) as a function of angles θ_{DOR1} and θ_{DOR2} (see Figure 3) was calculated, for each of the systems, from the history of the biasing hills applied to the simulation. Figure 3A reports the two-dimensional FES for the 4 dimer. As shown in this figure, there are two well-defined basins, *x* and *y*, exhibiting a free energy difference of ~6 kcal/mol. The ranges of angles (in degrees) for basin *x* are approximately as follows: 10.3° $\leq \theta_{DOR1} \leq$ 14.3°, and 5.7° $\leq \theta_{DOR2} \leq$ 12.6°. Basin *y* is approximately positioned at the following angles: 21.2° $\leq \theta_{DOR1}$

Table 1: Symmetrical Residues in Spatial Proximity (< 15 Å) and Facing One Another (the Cα−Cα distance longer than the Cβ−Cβ Distance) for Each of the Putative 4 or 4/5 Interfaces during a 1 ns Explicit Atomic Scale Simulation[a]

TM4		TM4 and TM5		Cβ−Cβ (Å)
K166	4.43	V188	EL2	< 7
I170	4.47	P191	EL2	
S177	4.54			
V181	4.58			
V185	4.62			
P162	4.39	V179	4.56	7
W173	4.50	R192	EL2	
V174	4.51			
A163	4.40	D158	IL2	8
		L175	4.52	
		I183	4.60	
				9
S126	3.30	C171	4.48	10
		G178	4.55	
		M186	EL2	
I86	2.41	T213	5.38	11
K122	3.26			
A123	3.27			
Q190	EL2			
G178	4.55	K164	4.41	12
T189	EL2	I168	4.45	
		F220	5.45	
N90	2.45	F159	IL2	13
		V217	5.42	
K81	IL1	K155	IL2	14
		G180	4.57	
		S206	EL2	

[a]The last column gives their average proximity (Cβ−Cβ) during the simulation.

≤ 26.9°, and 18.3° ≤ θ_{DOR2} ≤ 24.1°. This is in sharp contrast to Figure 3B, showing the FES for the 4/5 dimer. This FES shows little detail, i.e., little variation in energy across the available range of angles. We have selected a structure from a basin at the following values: θ_{DOR1} = 36.1° and θ_{DOR2} = 17.2°.

Structures were extracted from the basins described above, and example structures from the minima were reconstructed at atomic resolution for each dimer (see Materials and Methods for details). These structures were embedded into an explicit all-atom POPC/10% cholesterol membrane, solvated, and simulated for 1 ns, as described in Materials and Methods.

Figure S6A of the Supporting Information shows the distances among the DOR regions most involved in dimeric interaction calculated for the 4 dimer during a 1 ns simulation. The gray lines delimit the helices and loops. Contacts are colored gray if the distance between the Cβ atom of each residue is > 15 Å. Contacts at a Cβ−Cβ distance of < 15 Å are colored from blue to pink, with decreasing contact distance. The tightest interactions are shown along the full length of TM4, and between the C-terminal end of TM4 and the N-terminal end of TM3 to EL1. There are also several interactions of intracellular loop 2 (IL2), through TM4, with the C-terminal end of TM1 through IL1 to almost the full length of TM2.

Table 1 shows the symmetrical interprotomer contacts (distance between Cβ atoms of < 15 Å) between residues facing one another (i.e., the Cα−Cα distance longer than the Cβ−Cβ distance, indicating that Cβ atoms point toward one another in most residues, with the exception of glycines), during a 1 ns simulation of the atomistic reconstructions of structures extracted from the FES basins for each of the interfaces. In the 4 dimer, residues K166$^{4.43}$, I170$^{4.47}$, S177$^{4.54}$, V181$^{4.58}$, and V185$^{4.62}$ are all in the proximity of their symmetrical counterpart at the TM4 interface. These interactions are supported by other symmetrical interactions among TM3, TM2, and extracellular loop 2 (EL2). There is no clear predominance of any type of residue, e.g., hydrophobic or polar, over any other type in this interface. At first glance, some of the interactions may seem unexpected, for example, a symmetrical interaction between two lysine residues, as in the case of K166$^{4.43}$, but upon closer inspection, it is apparent that the side chains lie adjacent to one another and the charged regions interact with the backbone of residues on the opposite protomer, tightening the interface. The conserved tryptophan residues at the interface, W173$^{4.50}$, are oriented in a configuration that could support π−π stacking, which would also strengthen the interface.

Figure 4A shows the configurations representative of the lowest-energy basin identified for the 4 dimer of DOR, with residues that make up the interface (i.e., facing one another and within 15 Å of each other) color-coded according to their proximity, as listed in Table 1. We highlight only the residues from the TM and H8 regions for the sake of simplicity. Figure 4B shows the residues involved in interprotomer interaction in the 4/5 dimer. As reported in Table 1, the 4/5 dimer presents several symmetrical residues in spatial proximity along the length of TM4 and some in TM5, but the interprotomeric interface appears to be dominated by the spatial proximity of residues on EL2. The contact map for the most involved regions in this dimeric arrangement is shown in Figure S6B of the Supporting Information. From this map, it is clear that the interface is dominated by the extracellular region of the protomers, and that the helix−loop boundary regions of EL2 play a key role in the 4/5 dimer. Although bending toward the binding pocket of the receptor, both the N- and C-terminal ends of the EL2 loop protrude across the interface toward the other protomer (see Figure 4), hindering tighter packing between the helices deeper in the membrane and at the intracellular ends of the protomers.

Strength of Association of the 4/5 Dimer Compared to the 4 Dimer. To estimate the relative stability of the 4/5 dimer versus the 4 dimer, we performed umbrella sampling simulations of the CG 4/5 dimer in an explicit CG POPC/10% cholesterol environment and compared the results of these simulations with analogous simulations we recently conducted with the 4 dimer (*17*). As shown in Figure 5, a single minimum was identified for the 4/5 dimer (blue line) at an energy higher than those of the two energetically and structurally similar dimeric minima previously identified for the 4 dimer (red line) (*17*). Using the calculated free energy area for the 4/5 dimer from Figure 5 and the formalism originally described by Roux and co-workers (*47*−*49*) and recently applied by us to the 4 dimer of DOR (see details in ref *17*), we estimated a dimerization constant (K_{Dimer}) of ≅0.05 μm^2 for the identified lowest-energy 4/5 dimer compared to the recently reported value of 1.02 μm^2 for the 4 dimer (*17*). Using this dimerization constant in combination with a diffusion coefficient of 0.08 $\mu m^2/s$ determined experimentally for MOR (*15*), we calculated a half-time of 0.2 s for the 4/5 dimer, compared to the value of 4.4 s previously reported for the 4 dimer (*17*).

DISCUSSION

We have used disulfide cross-linking of endogenous and substituted cysteines to identify residues in TM4 and TM5 at

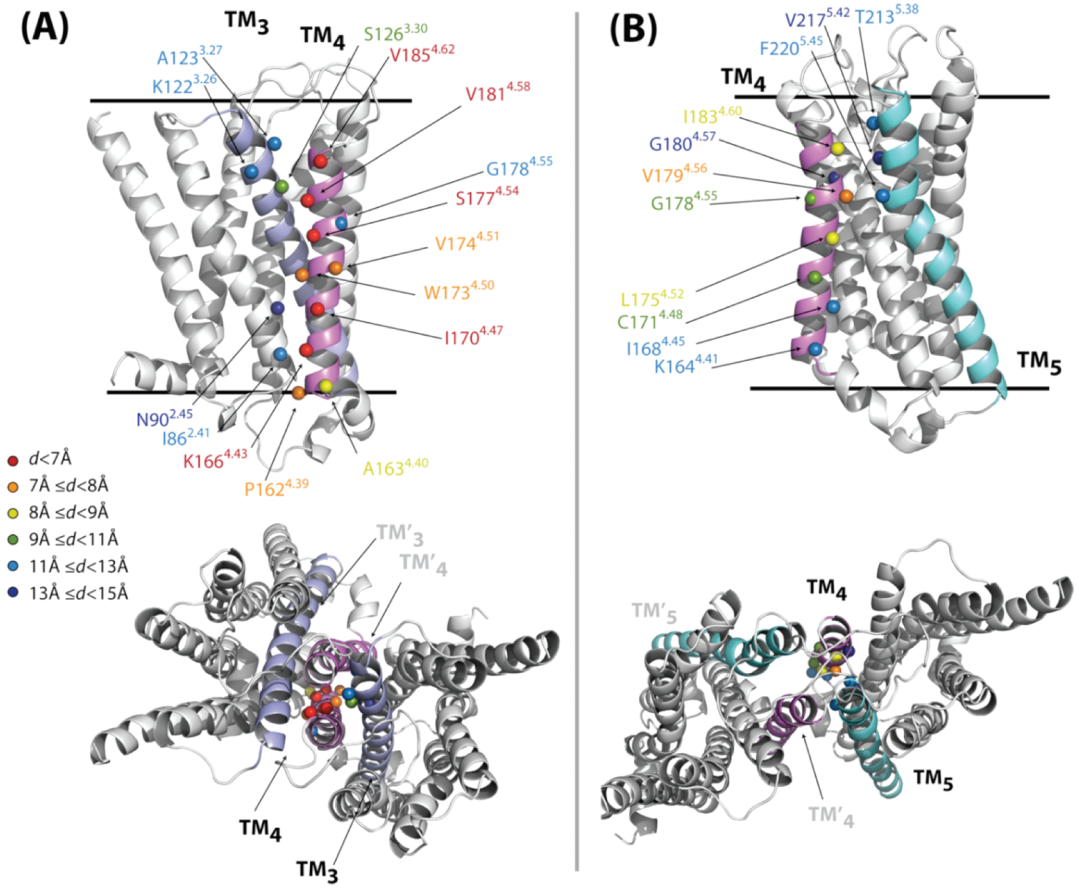

FIGURE 4: Residues at the 4 interface. (A, top) Residues of one protomer found to be within 15 Å of their symmetric partners on the other protomer, and facing each other. (A, bottom) Complete dimer as seen from the extracellular side. (B) Same information reported for the 4/5 interface. For the sake of clarity, only residues from the TM domain and H8 have been included.

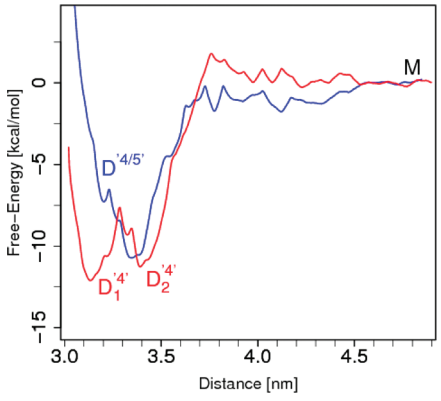

FIGURE 5: Free energy of 4 (red) or 4/5 (blue) interprotomeric arrangements of DOR restrained in their relative orientation by square-well potentials applied on the rotational angles. For the sake of simplicity, the curves are shifted to assign 0 values to monomeric states ($r \geq 4.5$ nm).

the interface of DOR homodimers. These findings were used to guide a total of 3 μs of well-tempered metadynamics CG simulations to characterize at the atomic level the putative interfaces between interacting protomers of the DOR. In accordance with predictions from correlated mutation analysis of ORs (*53*, *54*), and with published experimental evidence for several GPCR dimers and/or oligomers (*19*−*31*), we first focused on the TM4 and TM5 interfaces. We discovered that endogenous cysteines at positions 4.48 and 5.41 were cross-linked by $HgCl_2$ but not by CuP, consistent with the ability of $HgCl_2$ to penetrate deeper in the membrane and also with its ability to bridge more distant cysteines that might not collide directly. Removal of the three endogenous cysteines in TM1, TM4, and TM5 led to a pseudo-Cys-less DOR; treatment with $HgCl_2$ and CuP had no effect on the migration of DOR on nonreducing SDS−PAGE. This construct was used for subsequent cysteine substitution. Substitutions V181$^{4.58}$C and T213$^{5.38}$C at the extracellular ends of TM4 and TM5 led to cross-linking with both CuP and $HgCl_2$, providing further evidence of the role of these interfaces in DOR homomerization. These findings are in general agreement with our previous studies on D2R, which supported the direct involvement of lipid-exposed surfaces of TM4 and/or TM5 in dimerization/oligomerization interfaces (*21*, *22*). However, it is notable that the extent of cross-linking is lower in the DOR and the residues that cross-link are much more limited in contrast to the broad stripe of cross-linking detected in the D2R (*20*, *21*). Several residues in DOR such as G180$^{4.57}$, M184$^{4.61}$, M186$^{4.63}$, and I215$^{5.40}$ did not exhibit any appreciable cross-linking by CuP or $HgCl_2$ when mutated to cysteine, despite their predicted orientation on the same faces as V181$^{4.58}$ or T213$^{5.38}$. There are a number of potential explanations for this more limited cross-linking, including access of the reagents, the microenvironment and ionization state of the cysteine, and the possibility that the interfaces in the DOR may be more dynamic than that of the D2R.

To investigate further details of these dynamic interfaces, we explored the conformational space accessible to interacting DOR protomers centered at position 4.58 or 5.38. Our computational results point to energetically preferred configurations of the 4

dimer that are characterized by specific residue interactions. In line with the experiments, our computations are consistent with the proximity (< 7 Å) of V181$^{4.58}$ to its symmetrical counterpart, during a 1 ns unrestrained all-atom simulation of the predicted lowest-energy configuration of the 4 dimer in an explicit POPC/10% cholesterol/solvent environment. Other very close residues (< 8 Å) predicted to face each other at this TM4 interface are K166$^{4.43}$, I170$^{4.47}$, S177$^{4.54}$, V185$^{4.62}$, V174$^{4.51}$, W173$^{4.50}$, and P162$^{4.39}$. The free energy surfaces generated from the metadynamics calculations indicate that this proposed 4 dimer configuration of DOR corresponds to the lowest-energy minimum.

The free energy surface shown in Figure 3B for the 4/5 dimer indicates there is little variation across the range of angles representing this interface. Combined with the shorter lifetime calculated for the 4/5 dimer and the weaker cross-linking at position 5.38, as compared to those for the 4 dimer and the residue at position 4.58, these findings suggest that the 4 dimer interface is more specific than that of the 4/5 dimer. Unlike the case of the 4 dimer, the closest interactions between residues at the interface of the 4/5 dimer do not encompass the full membrane span of the protomers (from extra- to intracellular regions), thus contributing to its reduced stability. The calculated contact maps show that interfacial contacts in the 4/5 dimer are dominated by the (more flexible) helix−loop boundary regions for EL2, which might be expected to reduce the angle specificity, when compared to the 4 dimer interface where the interactions are predominantly helix−helix interactions.

Notably, our calculated lifetimes of DOR homodimers approximate the association and dissociation kinetics of M1 muscarinic receptors assessed by single-molecule studies (*12*). The lifetime of DOR homodimers appears to be relatively short. Although the strength of DOR dimerization appears to depend on the protein sequence at the interface, with the 4 dimer being more stable than the 4/5 dimer, we cannot rule out a contribution of other factors, such as the hydrophobic mismatch between the thicknesses of the receptor TM region and the lipid bilayer, to receptor interactions.

Our computational results are consistent with the data we obtained from cysteine cross-linking experiments conducted with DOR and might relate to the more limited cross-linking observed in DOR relative to D2R (*20*, *21*). To understand whether the nature of interaction is similar for all GPCR pairs, additional simulations on several different GPCR systems are currently ongoing in our lab.

SUPPORTING INFORMATION AVAILABLE

Additional details concerning the results obtained are provided. Figure S1 shows hill heights (left panels) indicating convergence of the simulations, as well as the bias applied during the simulations (right panels). Figure S2 depicts the results of BRET titration experiments. Figure S3 shows surface expression of mutants resulting from flow cytometry analysis. Figure S4 illustrates a flowchart of the modeling and simulation strategy. Panels A and B of Figure S5 show the time evolution of θ_{DOR1} (light gray) and θ_{DOR2} (dark gray) for the 4 and 4/5 dimers, respectively. Figure S6 reports contact maps of the protomeric regions most involved in the (A) 4 and (B) 4/5 dimeric arrangements calculated during 1 ns. The tables give details of the cross-linking results for each mutant construct with the two different reagents (Table S1), K_d and B_{max} values for delta opioid receptor WT and mutants obtained during saturation binding of [^{3}H]naltrindole in intact cells (Table S2), and SNC-80-induced activation of G protein by WT and key mutants, measured using a BRET biosensor (Table S3). This material is available free of charge via the Internet at http://pubs.acs.org.

REFERENCES

1. Dhawan, B. N., Cesselin, F., Raghubir, R., Reisine, T., Bradley, P. B., Portoghese, P. S., and Hamon, M. (1996) International Union of Pharmacology. XII. Classification of opioid receptors. *Pharmacol. Rev. 48*, 567–592.
2. Milligan, G. (2008) A day in the life of a G protein-coupled receptor: The contribution to function of G protein-coupled receptor dimerization. *Br. J. Pharmacol. 153* (Suppl. 1), S216–S229.
3. Gomes, I., Jordan, B. A., Gupta, A., Rios, C., Trapaidze, N., and Devi, L. A. (2001) G protein coupled receptor dimerization: Implications in modulating receptor function. *J. Mol. Med. 79*, 226–242.
4. Rutherford, J. M., Wang, J., Xu, H., Dersch, C. M., Partilla, J. S., Rice, K. C., and Rothman, R. B. (2008) Evidence for a mu-delta opioid receptor complex in CHO cells co-expressing mu and delta opioid peptide receptors. *Peptides 29*, 1424–1431.
5. Martin, N. A., and Prather, P. L. (2001) Interaction of co-expressed mu- and delta-opioid receptors in transfected rat pituitary GH_3 cells. *Mol. Pharmacol. 59*, 774–783.
6. Rios, C. D., Jordan, B. A., Gomes, I., and Devi, L. A. (2001) G-protein-coupled receptor dimerization: Modulation of receptor function. *Pharmacol. Ther. 92*, 71–87.
7. Gomes, I., Gupta, A., Filipovska, J., Szeto, H. H., Pintar, J. E., and Devi, L. A. (2004) A role for heterodimerization of mu and delta opiate receptors in enhancing morphine analgesia. *Proc. Natl. Acad. Sci. U.S.A. 101*, 5135–5139.
8. Milligan, G. (2005) Opioid receptors and their interacting proteins. *Neuromol. Med. 7*, 51–59.
9. Cvejic, S., and Devi, L. A. (1997) Dimerization of the delta opioid receptor: Implication for a role in receptor internalization. *J. Biol. Chem. 272*, 26959–26964.
10. McVey, M., Ramsay, D., Kellett, E., Rees, S., Wilson, S., Pope, A. J., and Milligan, G. (2001) Monitoring receptor oligomerization using time-resolved fluorescence resonance energy transfer and bioluminescence resonance energy transfer. The human delta-opioid receptor displays constitutive oligomerization at the cell surface, which is not regulated by receptor occupancy. *J. Biol. Chem. 276*, 14092–14099.
11. Wang, D., Sun, X., Bohn, L. M., and Sadee, W. (2005) Opioid receptor homo- and heterodimerization in living cells by quantitative bioluminescence resonance energy transfer. *Mol. Pharmacol. 67*, 2173–2184.
12. Hern, J. A., Baig, A. H., Mashanov, G. I., Birdsall, B., Corrie, J. E., Lazareno, S., Molloy, J. E., and Birdsall, N. J. (2010) Formation and dissociation of M1 muscarinic receptor dimers seen by total internal reflection fluorescence imaging of single molecules. *Proc. Natl. Acad. Sci. U.S.A. 107*, 2693–2698.
13. Dorsch, S., Klotz, K. N., Engelhardt, S., Lohse, M. J., and Bunemann, M. (2009) Analysis of receptor oligomerization by FRAP microscopy. *Nat. Methods 6*, 225–230.
14. Fonseca, J. M., and Lambert, N. A. (2009) Instability of a class a G protein-coupled receptor oligomer interface. *Mol. Pharmacol. 75*, 1296–1299.
15. Sauliere-Nzeh Ndong, A., Millot, C., Corbani, M., Mazeres, S., Lopez, A., and Salome, L. (2010) Agonist-selective dynamic compartmentalization of human mu opioid receptor as revealed by resolutive FRAP analysis. *J. Biol. Chem. 285*, 14514–14520.
16. Ballesteros, J. A., and Weinstein, H. (1995) Integrated methods for the construction of three-dimensional models and computational probing of structure-function relations in G protein-coupled receptors. *Methods Neurosci. 25*, 366–366.
17. Provasi, D., Johnston, J. M., and Filizola, M. (2010) Lessons from free energy simulations of delta-opioid receptor homodimers involving the fourth transmembrane helix. *Biochemistry 49*, 6771–6776.
18. Lambert, N. A. (2010) GPCR dimers fall apart. *Sci. Signaling 3*, pe12.
19. Lee, S. P., O'Dowd, B. F., Rajaram, R. D., Nguyen, T., and George, S. R. (2003) D2 dopamine receptor homodimerization is mediated by multiple sites of interaction, including an intermolecular interaction involving transmembrane domain 4. *Biochemistry 42*, 11023–11031.
20. Guo, W., Shi, L., Filizola, M., Weinstein, H., and Javitch, J. A. (2005) Crosstalk in G protein-coupled receptors: Changes at the transmembrane homodimer interface determine activation. *Proc. Natl. Acad. Sci. U.S.A. 102*, 17495–17500.

21. Guo, W., Shi, L., and Javitch, J. A. (2003) The fourth transmembrane segment forms the interface of the dopamine D2 receptor homodimer. *J. Biol. Chem. 278*, 4385–4388.
22. Guo, W., Urizar, E., Kralikova, M., Mobarec, J. C., Shi, L., Filizola, M., and Javitch, J. A. (2008) Dopamine D2 receptors form higher order oligomers at physiological expression levels. *EMBO J. 27*, 2293–2304.
23. Berthouze, M., Rivail, L., Lucas, A., Ayoub, M. A., Russo, O., Sicsic, S., Fischmeister, R., Berque-Bestel, I., Jockers, R., and Lezoualc'h, F. (2007) Two transmembrane Cys residues are involved in 5-HT4 receptor dimerization. *Biochem. Biophys. Res. Commun. 356*, 642–647.
24. Mancia, F., Assur, Z., Herman, A. G., Siegel, R., and Hendrickson, W. A. (2008) Ligand sensitivity in dimeric associations of the serotonin 5HT2c receptor. *EMBO Rep. 9*, 363–369.
25. Carrillo, J. J., Lopez-Gimenez, J. F., and Milligan, G. (2004) Multiple interactions between transmembrane helices generate the oligomeric α1b-adrenoceptor. *Mol. Pharmacol. 66*, 1123–1137.
26. Lopez-Gimenez, J. F., Canals, M., Pediani, J. D., and Milligan, G. (2007) The α1b-adrenoceptor exists as a higher-order oligomer: Effective oligomerization is required for receptor maturation, surface delivery, and function. *Mol. Pharmacol. 71*, 1015–1029.
27. Klco, J. M., Lassere, T. B., and Baranski, T. J. (2003) C5a receptor oligomerization. I. Disulfide trapping reveals oligomers and potential contact surfaces in a G protein-coupled receptor. *J. Biol. Chem. 278*, 35345–35353.
28. Hernanz-Falcon, P., Rodriguez-Frade, J. M., Serrano, A., Juan, D., del Sol, A., Soriano, S. F., Roncal, F., Gomez, L., Valencia, A., Martinez, A. C., and Mellado, M. (2004) Identification of amino acid residues crucial for chemokine receptor dimerization. *Nat. Immunol. 5*, 216–223.
29. Gonzalez-Maeso, J., Ang, R. L., Yuen, T., Chan, P., Weisstaub, N. V., Lopez-Gimenez, J. F., Zhou, M., Okawa, Y., Callado, L. F., Milligan, G., Gingrich, J. A., Filizola, M., Meana, J. J., and Sealfon, S. C. (2008) Identification of a serotonin/glutamate receptor complex implicated in psychosis. *Nature 452*, 93–97.
30. Gao, F., Harikumar, K. G., Dong, M., Lam, P. C., Sexton, P. M., Christopoulos, A., Bordner, A., Abagyan, R., and Miller, L. J. (2009) Functional importance of a structurally-distinct homo-dimeric complex of the Family B G protein-coupled secretin receptor. *Mol. Pharmacol. 76*, 264–274.
31. Mikhailova, M. V., Blansett, J., Jacobi, S., Mayeux, P. R., and Cornett, L. E. (2008) Transmembrane domain IV of the *Gallus gallus* VT2 vasotocin receptor is essential for forming a heterodimer with the corticotrophin releasing hormone receptor. *J. Biomed. Opt. 13*, 031208.
32. Han, Y., Moreira, I. S., Urizar, E., Weinstein, H., and Javitch, J. A. (2009) Allosteric communication between protomers of dopamine class A GPCR dimers modulates activation. *Nat. Chem. Biol. 5*, 688–695.
33. Hollins, B., Kuravi, S., Digby, G. J., and Lambert, N. A. (2009) The C-terminus of GRK3 indicates rapid dissociation of G protein heterotrimers. *Cell. Signalling 21*, 1015–1021.
34. Provasi, D., Bortolato, A., and Filizola, M. (2009) Exploring molecular mechanisms of ligand recognition by opioid receptors with metadynamics. *Biochemistry 48*, 10020–10029.
35. Cherezov, V., Rosenbaum, D. M., Hanson, M. A., Rasmussen, S. G., Thian, F. S., Kobilka, T. S., Choi, H. J., Kuhn, P., Weis, W. I., Kobilka, B. K., and Stevens, R. C. (2007) High-resolution crystal structure of an engineered human β2-adrenergic G protein-coupled receptor. *Science 318*, 1258–1265.
36. Sali, A., and Blundell, T. L. (1993) Comparative protein modelling by satisfaction of spatial restraints. *J. Mol. Biol. 234*, 779–815.
37. Wang, C., Bradley, P., and Baker, D. (2007) Protein-protein docking with backbone flexibility. *J. Mol. Biol. 373*, 503–519.
38. Marrink, S. J., Risselada, H. J., Yefimov, S., Tieleman, D. P., and de Vries, A. H. (2007) The MARTINI force field: Coarse grained model for biomolecular simulations. *J. Phys. Chem. B 111*, 7812–7824.
39. Monticelli, L., Kandasamy, S. K., Periole, X., Larson, R. G., Tieleman, D. P., and Marrink, S. J. (2008) The MARTINI coarse-grained force field: Extension to proteins. *J. Chem. Theory Comput. 4*, 819–834.
40. Hess, B., Kutzner, C., van der Spoel, D., and Lindahl, E. (2008) GROMACS 4: Algorithms for Highly Efficient, Load-Balanced, and Scalable Molecular Simulation. *J. Chem. Theory Comput. 4*, 435–447.
41. Bonomi, M., Branduardi, D., Bussi, G., Camilloni, C., Provasi, D., Raiteri, P., Donadio, D., Marinelli, F., Pietrucci, F., and Broglia, R. A. (2009) PLUMED: A portable plugin for free-energy calculations with molecular dynamics. *Comput. Phys. Commun. 180*, 1961–1972.
42. Kandt, C., Ash, W. L., and Tieleman, D. P. (2007) Setting up and running molecular dynamics simulations of membrane proteins. *Methods 41*, 475–488.
43. Barducci, A., Bussi, G., and Parrinello, M. (2008) Well-tempered metadynamics: A smoothly converging and tunable free-energy method. *Phys. Rev. Lett. 100*, 020603.
44. Bussi, G., Zykova-Timan, T., and Parrinello, M. (2009) Isothermal-isobaric molecular dynamics using stochastic velocity rescaling. *J. Chem. Phys. 130*, 074101.
45. Berendsen, H. J. C., Postma, J. P. M., van Gunsteren, W. F., and DiNola, A. (1984) Molecular dynamics with coupling to an external bath. *J. Chem. Phys. 81*, 3684–3690.
46. Rzepiela, A. J., Schafer, L. V., Goga, N., Risselada, H. J., De Vries, A. H., and Marrink, S. J. (2010) Reconstruction of atomistic details from coarse-grained structures. *J. Comput. Chem. 31*, 1333–1343.
47. Roux, B. (1999) Statistical mechanical equilibrium theory of selective ion channels. *Biophys. J. 77*, 139–153.
48. Allen, T. W., Andersen, O. S., and Roux, B. (2004) Energetics of ion conduction through the gramicidin channel. *Proc. Natl. Acad. Sci. U.S.A. 101*, 117–122.
49. Roux, B., Andersen, O. S., and Allen, T. W. (2008) Comment on "Free energy simulations of single and double ion occupancy in gramicidin A" [J. Chem. Phys. 126, 105103 (2007)]. *J. Chem. Phys. 128*, 227101 (author reply, p 227102).
50. Ramsay, D., Kellett, E., McVey, M., Rees, S., and Milligan, G. (2002) Homo- and hetero-oligomeric interactions between G protein-coupled receptors in living cells monitored by two variants of bioluminescence resonance energy transfer. *Biochem. J. 365*, 429–440.
51. Hastrup, H., Sen, N., and Javitch, J. A. (2003) The human dopamine transporter forms a tetramer in the plasma membrane: Cross-linking of a cysteine in the fourth transmembrane segment is sensitive to cocaine analogs. *J. Biol. Chem. 278*, 45045–45048.
52. Soskine, M., Steiner-Mordoch, S., and Schuldiner, S. (2002) Cross-linking of membrane-embedded cysteines reveals contact points in the EmrE oligomer. *Proc. Natl. Acad. Sci. U.S.A. 99*, 12043–12048.
53. Filizola, M., Olmea, O., and Weinstein, H. (2002) Prediction of heterodimerization interfaces of G-protein coupled receptors with a new subtractive correlated mutation method. *Protein Eng. 15*, 881–885.
54. Filizola, M., and Weinstein, H. (2002) Structural models for dimerization of G-protein coupled receptors: The opioid receptor homodimers. *Biopolymers 66*, 317–325.